Published in final edited form as:
Nat Neurosci. 2018 January ; 21(1): 33–40. doi:10.1038/s41593-017-0037-5.

Synaptotagmin-1 drives synchronous Ca^{2+} triggered fusion by C_2B domain-mediated synaptic vesicle-membrane attachment

Shuwen Chang[1,2], **Thorsten Trimbuch**[1,2], and **Christian Rosenmund**[1,2,*]

[1]Institut für Neurophysiologie, Charité - Universitätsmedizin, Berlin, Germany

[2]NeuroCure Cluster of Excellence Cluster, Berlin, Germany

Abstract

The synaptic vesicle (SV) protein Synaptotagmin-1 (Syt1) is the Ca^{2+} sensor for fast synchronous release. Biochemical and structural data suggest that Syt1 interacts with phospholipids and SNARE complex, but how these interactions translate into SV fusion remains poorly understood. Utilizing flash-and-freeze electron microscopy, which triggers action potentials (AP) with light and coordinately arrests synaptic structures with rapid freezing, we found synchronous release-impairing mutations in the Syt1 C_2B domain (K325, 327; R398, 399) to also disrupt SV-active zone plasma membrane attachment. Single AP induction rescued membrane attachment in these mutants within <10ms through activation of the Syt1 Ca^{2+} binding site. The rapid SV membrane translocation temporarily correlates with resynchronization of release and paired pulse facilitation. Based on these findings, we redefine the role of Syt1 as part of Ca^{2+}-dependent vesicle translocation machinery, and propose that Syt1 enables fast neurotransmitter release by means of its dynamic membrane attachment activities.

Introduction

Effective neuronal communication relies on transduction of presynaptic action potentials (AP) into synaptic vesicle (SV) fusion, which is synchronized to the millisecond. To account for the fast speed of synaptic transmission, a subset of SVs in nerve terminals morphologically attach (dock) to the presynaptic active zones (AZ)1 where they prime to achieve fusion competence that is readily releasable by an action potential2,3. These steps are thought to require the fusion machinery-neuronal soluble NSF-attachment protein receptor (SNARE) to form a complex that prepares the SVs for exocytosis1,4. The vesicular protein Synaptotagmin-1 (Syt1) is a Ca^{2+} binding protein that is essential for fast and synchronous fusion5–7. Syt1 consists of a transmembrane region followed by two cytosolic C_2 domains (C_2A and C_2B). The C_2 domains contain loops of acidic residues at its top that initially repel membrane interactions, but switch to membrane binding once Ca^{2+} ions are

*Correspondence and requests for materials should be addressed to C.R. (christian.rosenmund@charite.de).

Author Contributions: S.C. performed experiments, and analyzed data. T.T produced molecular reagents. S.C and C.R. designed the experiments and wrote the manuscript.

The authors declare no competing financial interests.

Europe PMC Funders Author Manuscripts

sandwiched between its acidic residues and the anionic membranes. This switch is thought to trigger vesicle fusion at extremely fast speed8–11.

Given the proposed role of Syt1 in interacting with membranes on Ca^{2+} triggering, Syt1 is presumed to carry out its function downstream of vesicle docking and priming. Indeed, examination of ultrastructure from chemically fixed Syt1-deficent synapses reveals apparently normal SV distribution at the active zone6,12. Similarly, priming as probed by hypertonic sucrose solution were unaffected on loss of Syt16,12. These contrast with observations from mouse chromaffin cells, where Syt1 deletion leads to a drastic reduction in membrane docking of large dense core vesicles13,14, and cognate effects on synaptic vesicles at *C. elegans*15 and drosophila neuromuscular junctions16. Recently, studies have begun to employ high-pressure-freezing, which allows preservation of cellular features in near-to-native state 1,17. As a result, re-examination of ultrastructure in Syt1-deficient hippocampal cultured neurons18 or slice cultures1 showed a reduction in membrane-attached vesicles accompanied with a drastic/or slight reduction in the number of vesicles in nerve terminals, suggesting an indirect effect of Syt1 in vesicle docking, likely due to an impairment of the SV recycling19. Therefore, whether Syt1 plays a role in regulating SVs position relative to the AZ membrane at mammalian synapses remains controversial.

Biochemical and structural function studies related to the side and bottom of the C2B domain have provided additional insights in Syt1's function. First, a stretch of four consecutive lysine residues (K324-K327) at the side of the Syt1 C_2B domain have been proposed to bind to the phosphatidylinositol (4,5)-biphosphate (PIP2) clustered on the plasma membrane20–22. Charge neutralization at these residues has been shown to strongly impair synchronous release23. Second, at the bottom face of the C_2B domain, two basic residues (R398, R399) have been shown to be essential for synchronous release and furthermore displayed membrane-binding activity in the absence of Ca^{2+} 24,25. These results have supported a model that suggests electrostatic membrane interaction at the bottom of the C_2B domain may preposition Syt1 to bridge the SV and plasma membranes together on Ca^{2+} triggering26.

Apart from membrane binding both basic regions also bind to the assembled SNARE complex25,27,28, which has led to additional models in which Syt1 prepares the release machinery for synchronous release through simultaneous interactions with the SNARE complex and membrane(s). While the orientation and association of Syt1 before and during fusion is not resolved, it is also unclear how these interactions drive the synchronous vesicle fusion. Based on Syt1's membrane binding properties, fusion may be initiated through membrane penetration10, membrane buckling29–31, formation of hemifused intermediate32 or membrane-membrane bridging25,26.

However, direct visualization of Syt1's function in changing the dynamic structures of SV-plasma membrane in synapses has been hampered by the limited accessibility and millisecond time scale of vesicle exocytosis33,34. Electron microscopy provides sufficient spatial resolution to potentially distinguish between different models, but the temporal resolution of traditional fixation methods is orders of magnitudes slower than vesicle exocytosis. To access fast actions of Syt1 after binding to Ca^{2+} with nanometer/millisecond

spatiotemporal resolution, we employed flash-and-freeze electron microscopy, which combines optogenetics that induces action potential firing with rapid freezing that arrests synaptic structures milliseconds after precisely timed AP induction34. Together with site-directed mutagenesis and electrophysiology, we simultaneously correlated the dynamics of membrane structure with the structural function of Syt1. We specifically asked how mutations at functionally crucial residues of the Syt1 C_2B domain affect the dynamic distribution of SVs and plasma membrane during exocytosis. Our results provide evidence that Syt1 synchronizes SV fusion by driving vesicles to the plasma membrane.

Results

Syt1 mediates basal vesicle-membrane attachment via its basic residues of C_2B domain

To link molecular mechanisms involving Syt1 to vesicle release on the millisecond time scale, we utilized charge-neutralizing and release synchronization disrupting mutations in three distinct regions of its C_2B domain. The affected sites were proposed in biochemical and structural experiments to bind to anionic lipids20,21,26 or the SNARE complex25,27, including a polybasic stretch consisting of four consecutive lysine residues (K324-K327) located at the side20,23, two arginine residues (R398, R399) at the bottom24,35 and the acidic residues of the Ca^{2+} binding site at the top (D309, D363, D365)36(Fig. 1A). The three mutant constructs (K325A, K327A; R398Q, R399Q; D309A, D363A, D365A) in addition to wild-type Syt1 full length (FL) were used to rescue Syt1 expression in primary mass-cultured hippocampal neurons derived from Syt1 knock-out (KO) mice using a lentiviral expression system. All Syt1 rescue constructs yielded similar expression levels of Syt1 compared to wild-type (WT) littermate synapses as assessed by quantitative immunocytochemistry analysis (Fig. S1A, B). We confirmed in separate experiments using electrophysiological recordings from autaptic neurons that the Syt1 FL construct completely rescued the evoked excitatory postsynaptic current (EPSC) amplitudes to the Syt1 WT level, whereas the rescues with the mutant constructs displayed severe impairments in synchronous release as previously reported (Fig, 1B, C)23,24,36.

To examine how Syt1 mutants affect the distance between SV and plasma membrane, neurons of Syt1 WT, KO, and KO expressing rescue constructs were rapidly frozen using a high-pressure freezer. Followed by freeze substitution and resin embedding, thin sections were examined by transmission electron microscopy (TEM)34. In resting WT excitatory synapses, the number of membrane attached vesicles i.e. the density of vesicles immediately adjacent to the AZ membrane (membrane to membrane distance < 5nm) was 1.92 ± 0.11 per 500 nm of AZ length (Fig1 D, I S2A), whereas Syt1 deficient synapses displayed a 35 % reduction in density (1.24 ± 0.1 vesicles per 500nm AZ; ***$p < 0.0001$; Fig. 1E, I, S2B). The impairment in membrane-attached vesicles did not however cause the significant accumulation of SVs in the 10-nm range (Fig S2F) that had been observed in Munc13 and SNARE complex deficient mutants1. Syt1 mutant deficient in Ca^{2+} binding (D309, 363, 365A) fully restored the vesicle number to the level of Syt1 FL rescue (2.17 ± 0.13 and 2.01 ± 0.14 vesicle per 500nm AZ; respectively; Fig. 1F, I, S2C), whereas the side polybasic region (K325, 327A) and the bottom basic residue (R398, 399Q) mutants failed to recruit vesicles to the membrane (1.01± 0.08 and 0.89 ± 0.08 vesicles per 500nm AZ; respectively;

***p < 0.001; Fig. 1G-I, S2D-E). This result suggests at resting synapses, Syt1 is required for maintaining the SV density in close proximity to the AZ membrane. This function does not require the Ca^{2+} binding top loop but the basic residues at the side (K325, K327) and in the bottom (R398, R399) of its C_2B domain.

A reduction in vesicle membrane docking has been observed in previous studies examining Syt1 deficient neurons, but those impairments were interpreted as an impairment of vesicle synthesis resulting in overall reduction in vesicle density in presynaptic terminal18. We therefore quantified the total number of SVs in the presynaptic terminal, but did not observe an alteration in their numbers either Syt1 KO synapses or mutant rescues compared to WT (Fig.1J, S3 A-I). In addition, we found that the total number of vesicles was not correlated to the number of docked vesicles (Fig. 2J). Thus, the impairment in vesicle membrane attachment is unlikely due to a secondary effect of loss of SVs in the terminals. In addition to the changes in vesicle docking caused by the Syt1 mutation, we found in electrophysiological recordings from the same mass-cultured preparation a similar modification of readily releasable vesicle pool (RRP) size in Syt1 WT, Syt1 KO and the 3 rescue mutant constructs (Fig S4), indicating that the alteration in vesicle membrane attachment parallels vesicle priming, consistent with the concept that membrane attachment is a prerequisite for vesicles to be primed1.

Syt1 mediates membrane attachment via its Ca^{2+} binding top loops of C2 domains

Next, as a sensor for fast Ca^{2+}-triggered release, Syt1 must execute its function during the Ca^{2+} triggering step. To capture the rapid action of Syt1 followed by AP-induced transient Ca^{2+} influx, we combined optogenetics with high-pressure freezing34, which elicits AP and arrests SVs within milliseconds after AP. A 10 ms pulse of blue light was applied to mass-cultured neurons of Syt1 WT, KO, and KO expressing rescue constructs and channelrhodopsin-2 (E123T/T159C; Cheta TC). The neurons were rapidly frozen 15 ms after light onset (approximately 10 ms after the light-induced AP; Fig. 1K). Comparing the distribution of SVs before and after a single AP in WT, we observed a 24% reduction in vesicles within 5 nm of the AZ (before: 1.92 ± 0.11; after AP: 1.45 ± 0.13 vesicles per 500nm AZ; **p < 0.01; Fig. 1D, L, S2A), demonstrating the unambiguous detection of AP/exocytosis mediated depletion of vesicles from the AZ34. Synapses from Syt1 KO and those rescued with the Syt1 C_2B top loop mutant (D309, 363, 365A) displayed no significant change in SV density at the AZ membrane after single AP stimulation (KO: before: 1.24 ± 0.1; after AP: 1.37 ± 0.16; Fig. 1E, L, S2B; D309, 363, 365A: before: 2.17 ± 0.13; after AP: 2.00 ± 0.18 vesicles per 500nm AZ; Fig. 1F, L, S2C), due to the fact that little or no fusion occurs within the first few milliseconds following stimulation in the mutants (Fig. 1B, C).

On the other hand, induction of a single AP surprisingly induced a rapid net movement of SVs towards the AZ in the two basic residue mutants, increasing vesicle density at the plasma membrane by 40% in neurons rescued by the K325, 327A mutant (before: 1.01 ± 0.08; after AP: 1.41 ± 0.1 vesicles per 500nm AZ; **p < 0.01; Fig. 1G, L, S2D) and 67% in the R398, 399Q mutant (before: 0.89 ± 0.08; after AP: 1.48 ± 0.14 vesicles per 500nm AZ, ***p < 0.001; Fig. 1H, L, S2E). This activity was blocked by addition of 250 μM Cd^{2+}

to the extracellular solution to prevent Ca^{2+} entry during depolarization, indicating this phenomenon is triggered by Ca^{2+} influx (Fig. 1L). As the Ca^{2+}-binding top loops are intact in both mutants, we hypothesized this AP/Ca^{2+}-activated membrane attachment activity may depend on the phospholipid binding ability of the Ca^{2+}-sensing top loops. To test this idea, we added additional mutations to the Ca^{2+} binding site of the C_2A and C_2B domains (Fig. 1L). As a control, basal membrane attachment was unchanged when the C_2A domain (D178, 230, 232A; termed 3DA) alone37 or combined C_2A and C_2B (D178, 230, 232A ; D309, 363, 365A; termed 6DA) were mutated in comparison to Syt1 WT (C_2A 3DA:1.82±0.14 and C_2AB 6DA:1.89±0.17 vs. WT:2.17±0.16 vesicles per 500 nm AZ; respectively; Fig. S5). In contrast, combining the Ca^{2+} binding site and basic residue mutants largely suppressed the Ca^{2+}-induced increase of SVs number after AP (Fig.1L). This suggests that Syt1 mediates Ca^{2+}-dependent SV-membrane attachment via its Ca^{2+} sensing loops. We name this activity Ca^{2+} dependent Syt1 docking.

Activity dependent Syt1 docking is transient and reversible

As Syt1 docking requires the binding of Ca^{2+}(Fig. 1L), we hypothesized that once Ca^{2+} fades away in the presynaptic terminal, the transient increase in vesicle docking should reverse. To test this, we examined SVs distribution of Syt1 R398, 399Q mutant expressing synapses at varied dwell times of 10, 100, and 500 ms after a single AP (Fig. 2A). Compared to resting condition, we found that Ca^{2+}-induced Syt1 docking was maximally enhanced 10 ms after the AP (161 ± 15 %; ** $p = 0.004$), partially reversed at 100 ms (115 ± 12 %) and completely reversed 500 ms after the AP (101 ± 14 %; *** $p < 0.001$; Fig. 2 B, C). This data suggests that the activity dependent Syt1 docking is transient and reversible, and likely related to the transient nature of the Ca^{2+} stimulus.

Transient Syt1 docking is required for synchronous vesicle fusion

Our results show the Syt1 C_2 domains control both Ca^{2+}-triggered Syt1 docking activity and synchronous release simultaneously, as best demonstrated in the Syt1 R398, 399Q mutant where both synchronous release and SV docking are impaired (Fig. 1B, C, I). We thus hypothesized that Syt1 docking is crucial for synchronous release. Based on the observation that AP-evoked Ca^{2+} influx partially restores the loss of membrane attached vesicle number in the Syt1R398, 399 mutants, we predicted AP-induced Syt1 docking should also boost synchronous release in subsequent synaptic responses as long as SVs were still docked. To probe for the link between Syt1 docking and synchronized vesicular release (Fig. 1L), we applied a pair of action potentials (10 ms apart) and compared the kinetics of the 1st and 2nd EPSC (Fig. 3A). Both Syt1 KO and R398, 399Q mutant showed an asynchronous first response and displayed synaptic facilitation. However, the magnitude of paired-pulse ratio (PPR) in R398, 399Q was 51% greater (KO: 3.7±0.2 vs. R398, 399Q: 5.6± 0.3; ***$p < 0.001$) (Fig. 3B, C). More importantly, the 2nd EPSC response from Syt1 KO neurons remained asynchronous, while the 2nd EPSC response in neurons expressing the R398, 399Q mutant became dramatically more synchronous (Fig. 3A, B). We analyzed the kinetics of evoked responses by fitting the response decay of the 2nd EPSC Syt1 KO and R398, 399Q mutant expressing neurons with double-exponential function and calculated the weighted decay time constant. The speed of release in the R398, 399Q mutant was selectively boosted

by the preceding AP, leading to 50% acceleration in the time constant. (1st EPSC: 98 ± 10 ms; 2nd EPSC: 49 ± 3 ms; ***p < 0.001; Fig. 3D, E, Supplementary Table 1F, G).

Time course of release synchronization matches the dynamic membrane attachment activity of Syt1

To further link Syt1 docking with synchronized release, we tested whether the time course of boosted synchronicity of release in the R398, 399Q mutant matches the transient time course of Ca^{2+}induced Syt1 docking. We applied sequential pairs of APs with variable inter-pulse intervals between the 1st and 2nd stimulus ranging from 10 ms – 500 ms to measure the release decay (Fig. 3F). We found that the response synchronicity was again largest at the shortest inter-pulse interval tested (10 ms; 194 ± 10%) and gradually became more asynchronous again. The decay time course of synchronization fitted well with a single exponential (**τ**= 56 ms **(**Fig. 3G). We also defined the decay time constant of short-term synaptic facilitation and found that facilitation was maximal at 10 ms interval (5.8 ± 0.3) and relaxed again at 500 ms (1.5±0.1) with a time constant similar to that for synchronization and Syt docking (**τ**= 46 ms). The similarity of the three time constants (Fig. 3G) provides a strong link between these three events. To test the relative contribution of Syt1-mediated docking activity to synaptic facilitation, we obtained the facilitation time constant in the Syt1 deficient neurons, which was 34 ms, emphasizing the importance of the intra-terminal Ca^{2+}transient as likely common link.

Release synchronization in the Syt1 R398, 399Q mutant depends on Ca^{2+}concentration

The transient effect in synchronization appeared largely dependent on Ca^{2} influx, we thus aim to define the Ca^{2+} sensitivity of Syt1 mediated release synchronization. We tested the paired-pulse behavior (10 ms apart) in the R398, 399Q mutant at varying external Ca^{2+} levels (1, 2, 4, and 10 mM Ca^{2+}) and quantified release kinetics of the 2nd EPSC of the responses (Fig. 3H-K). An acceleration of release speed occurred on elevation of Ca^{2+} level, showing a ~45% faster decay time constant when switching external Ca^{2+} from 2 mM to 4 mM (51 ± 5.9 ms to 28 ± 2.6 ms; respectively; ***p < 0.001; Fig. 3K) whereas the decay time constant remained the same in the wild-type FL rescue (Fig. 3H,I). The increase in release speed reached apparent saturation at 10 mM external Ca^{2+} with a time constant of 23 ± 2.3 ms (Fig. 3I). However, this was still slower than release synchronization of Syt1 WT FL rescue (10 ± 0.8 ms; Fig. 3I, J,K), consistent with a partial rescue of the SV membrane attachment following AP induction in the Syt1 R398, 399Q mutant (Fig.1L, Table S1C). Interestingly, the power relationship between release kinetics and extracellular Ca^{2+} concentration was steep, with a half-maximal effective concentration of 3.11 mM and a Hill slope of 4.2 (Fig. 3I). It suggests not only that the magnitude of release but also the degree of synchronization take place in a highly Ca^{2+} cooperative manner, likely resulting from either multiple Syt1 proteins or multiple Ca^{2+} ions engaging with the release machinery in concert38. Given our general observation that SV-membrane attachment is linked to release synchronization, we plotted the relative release rate as a function of the membrane attachment activities from the experiments in Fig 1I, 2C, 3G to describe the nature of the correlation. We found that synchronization was ~2-fold increased 10 ms after AP in the R398, 399Q mutant, while decay rate was ~10-fold faster in wild-type FL than that in R398, 399Q mutant rescued neurons (Fig. 3L). Thus, single AP did not completely rescue the

membrane attachment activity of R398, 399Q mutant to the wild-type level, similarly to the synchronicity. Furthermore, the relationship between release synchronicity and SV membrane distance seemed nonlinear (Fig. 3L). This result strongly emphasizes the role of SV-membrane distance in the speed of neurotransmitter release and provides a compelling model for how Syt1 exerts its action as a sensor for fast Ca^{2+} triggered release.

Syt1 works in concert with SNARE complex-mediated vesicle docking

Syt1 can both interact both with membrane phospholipids and the SNARE complex via its C_2 domains.25,27,29 Syt1-SNARE complex interactions are also thought to be crucial to couple the Syt1-Ca^{2+}-sensing function to membrane fusion during neurotransmitter release. To investigate whether transient Syt1 docking requires an assembled SNARE complex, we employed BoNT/A toxin, which cleaves the last C-terminal 9 amino acids of SNAP-2539 (Fig. S6A,B), and BoNT/B, which cleaves at the 76^{th} amino acid of VAMP/Synaptobrevin-2,40 to impair (in the former case) or block (in the latter case) trans-SNARE complex formation. Treatment of BoNT/A or BoNT/B overnight led to complete loss of synaptic responses (Fig. 4D, E) without affecting light-induced AP generation (Fig. 4A, B) as probed by electrophysiology recordings of mass-cultured Syt1 WT neurons expressing channelrhodopsin-2 variant (ChetaTC). We then subjected BoNT/A or BoNT/B- treated WT neurons to a single AP stimulation and froze them within 15 ms after light onset. The rationale was that if Ca^{2+}-induced Syt1 docking is independent of SNARE complex assembly, toxin treatment should not impair AP-induced increases in vesicle docking. However, ultrastructure analysis revealed no significant changes in vesicle distribution after single AP in either condition (Fig. 4G-J), suggesting that activity-dependent Syt1 docking requires full SNARE complex assembly.

While quantifying the docked vesicle number of toxin-treated synapses at rest, we observed that cleavage of the C-terminal of SNAP-25 with BoNT/A only led to a 25% reduction in docked vesicle number in comparison to WT synapses (1.3 ± 0.09 vesicles per 500nm AZ; $^{*}p < 0.05$; Fig. 4C, F, G) whereas loss of functional VAMP via BoNT/B treatment abolished vesicle docking (0.31 ± 0.04 vesicles per 500nm AZ; $^{***}p < 0.001$) to a similar level as genetic loss of SNARE proteins including Syntaxin1, SNAP-25 or Synaptobrevin-2 (Fig. 4C,F,I)1. These observations suggest that partial SNARE complex assembly still permits SNARE complex-based vesicle docking, while it does not permit Syt1 dependent docking and synchronous release. Our data suggest that Syt1-mediated docking activity works in concert with docking induced by SNARE complex assembly.

Discussion

How Syt1 contributes to synchronous release remains a major question in the field of synaptic transmission. Our study provides evidences that Syt1 acts as a catalyst in SV-AZ membrane attachment. Firstly, we found at resting synapse, Syt1 is crucial to maintain SV density at the proximity of AZ. This action does not involve its Ca^{2+} binding, but requires its polybasic region and bottom residues, supporting the hypothesis that Syt1 might function as a SV tether during or prior to SNARE complex nucleation. Secondly, we found Syt1-mediated interactions are highly dynamic, following the transient nature of Ca^{2+} and

occurring with onset times of less than 10 ms (limited by the instrumentation) and offset times of 30-50 ms (Fig 2,3). Thirdly, we found these interactions require an at least partially assembled SNARE complex, with Syt1 working in concert with the SNARE-mediated "prime-docking" step (Fig.4, S4), which prepares SVs for fusion. Finally, our results demonstrate that Syt1-mediated SV membrane attachment largely correlates to synchronization of release. Therefore, we define the novel Syt1 dependent activity as "sync-docking" (Fig. 2, 3; Fig. S4). Our results emphasize that close range 0–5 nm interactions of membranes are crucial for efficient and rapid fusion. This may be due to the large energy barriers linked to the repulsive forces between the two-phospholipid membranes2 or to the transition of partial to fully zippered SNARE complexes41. It is also possible that Syt1 mediated membrane interactions promote the formation of energetically favorable membrane intermediates such as hemifused bilayers42.

Our work also contributes to the discussion of the relationship of vesicle docking and vesicle priming. Recent studies have suggested that morphological synaptic vesicle docking to the AZ membrane is the functional and molecular equivalents of vesicle priming and formation of the trans-SNARE complexes1,17. However, this fundamental observation is at odds with studies showing that vesicle priming in Syt1 KO is not altered6,43. We thus re-examined how vesicle priming correlates to our ultrastructural analyses. In contrast to previous studies6,12,43, we found a 62% reduction in readily RRP size in mass-cultured Syt1 KO synapses (Fig. S4). This reduction in RRP size was also found in K325, 327A and R398, 399Q C_2B mutants that displayed impaired basal vesicle docking activity (Fig. 1I). The results reinforce the notion that functional priming is equivalent to morphological docking. As such, we conclude that Syt1 is not in fact only a "postpriming" factor. We reason that the apparent discrepancy between our findings and those of others12,43 may derive from the difference in experimental protocol used by these studies, specifically, the inclusion of an atypically long hypertonic solution application (20~30 seconds) was employed. This might have led to a vast overrepresentation of primed vesicles. The latter are usually released within 1-2 s of the onset of hypertonic solution, while all subsequent release activities are vesicle refilling related44.

We demonstrate that close range 0-5 nm interactions of membranes are crucial for the release efficiency, but the question of how Syt1 mediated these close-range interactions remains. We favor a scenario previously postulated2, in which the assembled SNARE complex limits the movement of SVs to distances of 0–10 nm45, with the vesicles rapidly fluctuating within this range. Rather than acting as "glue", Syt1 helps to reduce the mean distance through short-lived interactions via the basic residues of Syt1 C_2B and the target membrane in the absence of Ca^{2+}(Fig. 1I). This phenomenon would explain why loss of Syt1 function leads to a complete loss of synchronous release and yet "only" a 35% reduction in the number of membrane attached vesicles as assayed in the electron microscopy (Fig. 1D, E, I). Within milliseconds after AP stimulation, Ca^{2+} influx transiently induces a second membrane docking event, now mediated by the Ca^{2+} binding sites, which then initiate synchronous release (Fig. 1L, 3A, S2A, E). These two modes of Syt1-dependent docking are not functionally equivalent, because disrupting the Syt1 Ca^{2+}-binding sites still permits Syt1 mediated membrane attachment at rest (Fig. 1I, Fig. S2), but blocks synchronous release (Fig. 1B,C). However, Ca^{2+}-dependent Syt1 docking qualitatively

substitutes for constitutive membrane docking mediated by the basic residues and allows subsequent synchronous release (Fig. 3).

In line with this concept, Ca^{2+}-dependent Syt1 docking may also contribute to short-term synaptic facilitation, a well-known phenomenon, in which synaptic strength is increased in response to preceding AP events46. A major contribution of facilitation is the elevation of bulk Ca^{2+} concentration, which in turn, affects Ca^{2+} sensor occupation46. However, it is tempting to speculate that the Ca^{2+} influx also “primes” SVs by attaching them to the membrane in a Syt1-dependent manner, which in turn leads to an enhanced synaptic response in the subsequent AP. Indeed, the time course of paired pulse facilitation and transient SV vesicle docking induced by a single AP (Fig. 3G) is remarkably similar.

Apart from the two modes of Syt1 mediated vesicle plasma membrane attachment, it is worth noting that all three sites of the C_2B domain that are involved in this function are also critically involved in synchronous release. Given the orientation of these sites in relation to each other25,27 (Fig. S7), it is likely that Syt1-mediated constitutive docking likely represents the simultaneous interactions of Syt1 with the SNARE complex and either the vesicle or plasma membrane. This triangular action of the C_2B domain is supported by our finding that mutating either R398, R399 or K325, K327 in the C_2B domain leads to an interruption of Ca^{2+}-independent constitutive Syt1 docking activity. On the triggering of Ca^{2+}, Syt1 additionally interacts with the second membrane through its Ca^{2+}-bound top loops10,11. Although which of the Syt1 basic sites interact with the membrane and which with the SNARE complex is still under debate25,27, we provide models that explain how Syt1 C_2B could orientate itself during the fusion process (Fig. S7). Regardless of the outcome, these interactions seem to optimize the orientation of the C_2B to bring the Ca^{2+} binding residues into an ideal position for targeting the membrane on Ca^{2+} triggering.

In summary, our data lend weight to previous protein-structure based studies on Syt1 and provide new insight into how Syt1 accelerates membrane fusion by bringing the synaptic vesicle and plasma membrane together before and on Ca^{2+} influx.

Online methods

Animal maintenance and generation of mouse lines

Animals were handled according to the regulations of Berlin authorities and animal welfare committee of the Charité – Universitätsmedizin Berlin, Germany under license no. 0220/09. Synaptotagmin-1 WT ($Syt1^{+/+}$) and KO ($Syt1^{-/-}$) mice on a C57BL/6 background were generated by interbreeding heterozygous mice as described previously24; each breeding cage contained 2 females and 1 male. Animals were kept in a specific-pathogen-free environment and in an individually ventilated cage system with a 12-h dark/light cycle.

Lentivirus constructs

Synaptotagmin-1 full length and point mutation constructs were generated from a mouse Syt1 cDNA (NCBI reference sequence: NM_001252341). The cDNA was cloned into a lentiviral vector with a human synapsin-1 promoter after a nuclear localization signal (NLS)-

RFP-P2A expression cassette as a reference for expression level. Viral particles were produced as described47.

Cell culture and lentivirus infection

Hippocampal neurons derived from postnatal day 0 (P0) Syt1 WT and KO of both sexes were used and plated at a density of 20k-30k cells/cm^2 on top of astrocytes feeder layer on 10 mm coverslips for electrophysiology recordings or 6 mm sapphire disks for high pressure freezing experiments. Astrocytes were plated one week before seeding neurons to generate a feeder layer. For autaptic cultures, neurons were plated at density of 300 cells/cm^2 on the micro islands of astrocytes as described.24 Neurons were infected with different rescue constructs and/or co-infected with channelrhodopsin-2 variant (E123T/T159C; ChetaTC) 24-48h after plating.

Immunocytochemistry

Neurons were fixed at DIV 14-16 with 4% paraformaldehyde (PFA) for 15 mins, washed, permeabilized with 0.1% PBS-Tween20 and further blocked in 5% normal goat serum. Monoclonal mouse antibody anti-Synaptotagmin-1 (1:1000; Synaptic System 105011), polyclonal chicken anti-MAP2 (1:2000; Chemicon AB5543), polyclonal guinea pig anti-Synaptophysin-1 (1:1000; Synaptic System 101004) and polyclonal guinea pig anti-Vglut1 (1:4000; Synaptic System 135304) were further used to confirm the localization and expression level of Syt1 and Syt1 mutants in the presynaptic terminals. For testing the cleavage of SNAP-25 by BoNT/A, monoclonal mouse anti-SNAP-25 (1:1000; Synaptic System 111111) and polyclonal rabbit anti-SNAP-25 (1:1000; Synaptic System 111002) were used to recognize the N-and C-terminal of the SNAP-25. Secondary antibody conjugated with Alexa Fluor 405 (Jason 703475155), 488 (Jason 706545148 and 715545151), 647 (715605151) or rhodamine-conjugated antibodies (Jackson 706295148) 1:1000 were used to visualize immunofluorescence. Images were acquired by using a spinning disc confocal system (Nikon CSU-X) with a 60x, 1.4 NA oil-immersion objective. Overexposure and photo bleaching were avoided by checking for saturation in synaptic boutons. Consistent exposure times were used for each channel per experiment. Z-stacks of neurons were set with a 0.5 μm inter-stack interval and total z-axis range of 3-4 μm, and a sum of intensity projection was further used for analyses. Quantification of Syt1 signals over Synaptophysin signals was performed using automated software “ImageJ” (National Institute of Health, Bethesda, MD) with built-in macros. Synapses (region of interest; ROI) were defined as Synaptophysin or Vglut1 positive signals, and the fluorescence intensity of Syt1 or SNAP-25 was then measured in the defined ROI. Relative expression level of Syt1 or SNAP-25 among groups was calculated by normalizing the measured intensities of Syt1 or SNAP-25 to that of Synaptophysin. The synapse densities were quantified by counting the number of Vglut1 positive puncta over the dendrite length with MAP2 positive staining. 5-10 images were collected per condition per culture, resulting in total 20-22 images for statistical analysis.

High-pressure freezing and two-dimensional electron microscopy

Cultured neurons grown on the sapphire disks were frozen at DIV 14-16 using a high-pressure freezer (HPM 100 Leica, Germany) with an integrated light stimulation device

under a pressure of 2100 bar. Prior to freezing, sample were mounted in an environment chamber (Leica, Germany) at temperature of 35°C in pre-warmed extracellular solution containing the following (in mM): 140 NaCl, 2.4 KCl, 10 HEPES, 10 glucose, 4 $CaCl_2$ and 2 $MgCl_2$ (~300 mOsm; pH 7.4) with 30 μM bicuculline and 3μM NBQX or additional 250 μM Cd^{2+}. Optical stimulation with energy density 6.2 mW/mm^2 was provided by a 470 nm LED (Schott, Germany). We applied a 10 ms blue light pulse to generate single AP. To assess the effect induced by fast Ca^{2+} transient with millisecond precision, we set the device to apply light stimulation 15 ms prior to freezing. Due to the temporal fluctuation for channelrhodopsin (Cheta TC)-triggered action potential (AP) (Averaged AP generation latency: 4.8 ± 0.4 ms)34, and the minimum time measured for the freezer to cool chamber from 35°C to target temperature -20°C (8 ms)34 we chose 15 ms as the freeze point as the events of interest occur approximately 10 ms after the action potential34. Following a freeze-substitution protocol as described34, samples were embedded in EPON. We randomly selected approximately 2-6 mm^2 areas containing cells from EPON embedded samples, sectioned at 40-70 nm thickness using an Ultracut UCT ultramicrotome (Leica, Germany), and collected on Formvar-coated (0.5%) 200-mesh copper grids. Thin sections were counterstained with 2% uranyl acetate and 0.3% lead citrate in distilled H_2O. Samples were further examined blindly with a FEI Tecnai G20 transmission electron microscope operated at 80-200 keV accelerating voltage. Electron micrographs (2048x2048 pixels) of synapses were captured based on a prominent asymmetric postsynaptic density (PSD) and a cluster of SVs with a Veleta CCD camera (Olympus, Germany) at 55,000-fold (pixel size: 0.71 nm) and 89,000-fold magnification (pixel size: 0.47 nm). Each electron micrograph usually contained a single synapse, and only excitatory synapses were included in the analyses. However, we could not completely exclude inhibitory synapses. Data were further subjected to blind analyses– here we employed a software developed for image J as reported by Watanabe et. al34 , which allows manual tracking of each SV in the synaptic terminal. We analyzed the number of total SVs, synapse area, active zone length (defined by PSD length) and the distance of each SV relative to the AZ in the electron micrograph. The distance of each SV to the AZ was measured by calculating the distance from the outer leaflet of the SV membrane to the inner leaflet of the AZ membrane with a specially developed macro for Matlab34. The overall distribution of SVs in each electron micrograph was then obtained by plotting the absolute number or cumulative number as a function of distance to the AZ membrane. Docked vesicles were defined as those directly in contact with the plasma membrane. The number of vesicles was normalized to the length of active zone length, where the total numbers of SVs were normalized to the synapse area. Data were obtained from at least three or more independent neuronal cultures with total sample size 100-250 (electron micrographs/synapses) for each condition. For detailed overview of the number of electron micrographs analyzed for each experiment, see figure legends and Supplementary Table 1.

Electrophysiology

Whole cell patch-clamp recording was performed on autaptic or mass cultured hippocampal neurons at DIV 13-18. All electrophysiological recordings were obtained at room temperature (~25°C) with a Multiclamp 700B amplifier controlled by Clampex10 software. Data were digitally sampled at 10 kHz and were filtered using a low-pass filter at 3 kHz

(Molecular Devices, California, USA). Off-line analysis was performed using Axograph X (Axograph Scientific, Sydney, Australia). The extracellular solution contained (in mM): 140 NaCl, 2.4 KCl, 10 HEPES, 10 glucose, 4 $CaCl_2$ and 2 $MgCl_2$ (~300 mOsm; pH 7.4). Pipettes with resistance (3-5 MOhm) were filled with intracellular solution containing (in mM): 136 KCl, 17.8 HEPES, 1 EGTA, 4.6 $MgCl_2$, 4 ATP-Na_2, 0.3 GTP-Na_2, 12 creatine phosphate and 50 U/ml phosphocreatine kinase (~300 mOsm; pH 7.4). Access resistance was compensated by 70%, and during recordings, neurons were clamped at -70 mV during recordings. Single action potentials (AP) were evoked by a 2 ms depolarization step to 0 mV and postsynaptic currents (EPSC) were recorded. Paired-pulse recordings were obtained by applying a second depolarization step with varied inter-pulse intervals including 10, 25, 50, 100 and 500 ms. In the calcium dependent synchronization assay, recordings were performed by application of extracellular solutions containing 1, 2, 4, or 10 mM $CaCl_2$ with 1mM $MgCl_2$ each. Readily releasable pool (RRP) size was measured by applying hypotonic solution (500 mM sucrose in extracellular solution containing 0.1 μM TTX plus additional 30 μM bicuculline to isolate the current from excitatory synapses) onto the cell using a fast-flow system with a rapid solution exchange time constant (20-30 ms). We used a short sucrose protocol with 5 second application duration. A transient inward current lasting 2~3 seconds followed by a steady-state current was acquired, ensuring vesicle refilling and release reached equilibrium. The RRP was then measured with the steady-state current set as baseline and then integrating the charge over the transient curve. For light stimulation experiment, optical stimulation with energy density 0.64 mW/mm^2 was provided by a 470 nm LED coupled into the fluorescence port of the microscope (Olympus-IX51) with a 20x objective and triggered by a TTL signal. For botulinum toxin (BoNT) experiments, 10 nM BoNT/A or BoNT/B (Miprolab, Göttingen, Germany) were applied to the medium of WT cultured neurons 16 hours prior to recording. A single 10 ms light pulse was sent to elicit single AP where the AP waveforms were recorded in current-clamp mode, and postsynaptic currents were monitored in voltage-clamp mode. The weighted decay time constant (τ) of the EPSCs was analyzed by fitting with double exponential functions of $EPSC_{fit}$ (t) = $Amplitude1\exp(-t/\tau_1) + Amplitude2\exp(-t/\tau_2)$. Synchronicity was defined as the charge ratio of the first and the second 10 ms of the EPSC response (Charge2nd 10ms/Charge1st 10ms). The synchronicity ratio was calculated by dividing the charge ratio of the 2nd EPSC by the 1st EPSC. Standard Hill equation dose response curve $Y = M/[1+(K_d/X]^n]$ was used to fit the Ca^{2+} does response for EPSC decay time constant. M is the maximum response, Kd is the dissociation constant, and n is cooperativity.

Statistics

Data summation and statistical analyses were performed using Prism (GraphPad, California, USA). All data were firstly subjected to D'Agostino and Pearson omnibus normality testing. Two-tailed unpaired Student's t-test or one-way ANOVA test for normally distributed data and Mann-Whitney test or Kruskal-Wallis ANOVA test for non-normally distributed data were then carried out. Dunn's or Dunnett's *post hoc* multiple comparison methods were used following ANOVA test, as indicated in the figure legends. Significance and P values were calculated and are shown in Supplementary Table 1. Data were acquired and analyzed in a blinded fashion and differences between data sets were considered insignificant at P values > 0.05. No statistical methods were used to predetermine sample sizes, and no

randomization was applied, but our sample sizes are similar to those reported in previous publications.1,24

Data availability

The data supporting the findings of this study are available from the corresponding author on reasonable request.

Supplementary Material

Refer to Web version on PubMed Central for supplementary material.

Acknowledgments

We thank Andrew Plested, Melissa Herman, Josep Rizo, Craig Garner and Thomas Südhof for discussions and comments on the manuscript, Shigeki Watanabe and Erik Jorgensen for technical support, the Charité viral core facility for virus production and Berit Söhl-Kielszinski for sample preparation. This work was supported by ERC grant SynVGLUT, Berlin Institute of Health, Stiftung Charite, German Research Council grants SFB958, Ro1296/7-1 and TRR186.

References

1. Imig C, et al. The morphological and molecular nature of synaptic vesicle priming at presynaptic active zones. Neuron. 2014; 84:416–431. DOI: 10.1016/j.neuron.2014.10.009 [PubMed: 25374362]
2. Jahn R, Fasshauer D. Molecular machines governing exocytosis of synaptic vesicles. Nature. 2012; 490:201–207. DOI: 10.1038/nature11320 [PubMed: 23060190]
3. Sudhof TC. The synaptic vesicle cycle. Annu Rev Neurosci. 2004; 27:509–547. DOI: 10.1146/annurev.neuro.26.041002.131412 [PubMed: 15217342]
4. Sudhof TC. Neurotransmitter release: the last millisecond in the life of a synaptic vesicle. Neuron. 2013; 80:675–690. DOI: 10.1016/j.neuron.2013.10.022 [PubMed: 24183019]
5. Brose N, Petrenko AG, Sudhof TC, Jahn R. Synaptotagmin: a calcium sensor on the synaptic vesicle surface. Science. 1992; 256:1021–1025. [PubMed: 1589771]
6. Geppert M, et al. Synaptotagmin I: a major Ca2+ sensor for transmitter release at a central synapse. Cell. 1994; 79:717–727. [PubMed: 7954835]
7. Fernandez-Chacon R, et al. Synaptotagmin I functions as a calcium regulator of release probability. Nature. 2001; 410:41–49. DOI: 10.1038/35065004 [PubMed: 11242035]
8. Mackler JM, Drummond JA, Loewen CA, Robinson IM, Reist NE. The C(2)B Ca(2+)-binding motif of synaptotagmin is required for synaptic transmission in vivo. Nature. 2002; 418:340–344. DOI: 10.1038/nature00846 [PubMed: 12110842]
9. Sutton RB, Davletov BA, Berghuis AM, Sudhof TC, Sprang SR. Structure of the first C2 domain of synaptotagmin I: a novel Ca2+/phospholipid-binding fold. Cell. 1995; 80:929–938. [PubMed: 7697723]
10. Chapman ER, Davis AF. Direct interaction of a Ca2+-binding loop of synaptotagmin with lipid bilayers. J Biol Chem. 1998; 273:13995–14001. [PubMed: 9593749]
11. Fernandez I, et al. Three-dimensional structure of the synaptotagmin 1 C2B-domain: synaptotagmin 1 as a phospholipid binding machine. Neuron. 2001; 32:1057–1069. [PubMed: 11754837]
12. Bacaj T, et al. Synaptotagmin-1 and -7 Are Redundantly Essential for Maintaining the Capacity of the Readily-Releasable Pool of Synaptic Vesicles. PLoS Biol. 2015; 13:e1002267.doi: 10.1371/journal.pbio.1002267 [PubMed: 26437117]
13. de Wit H, et al. Synaptotagmin-1 docks secretory vesicles to syntaxin-1/SNAP-25 acceptor complexes. Cell. 2009; 138:935–946. DOI: 10.1016/j.cell.2009.07.027 [PubMed: 19716167]

14. Kedar GH, et al. A Post-Docking Role of Synaptotagmin 1-C2B Domain Bottom Residues R398/399 in Mouse Chromaffin Cells. J Neurosci. 2015; 35:14172–14182. DOI: 10.1523/JNEUROSCI.1911-15.2015 [PubMed: 26490858]
15. Jorgensen EM, et al. Defective recycling of synaptic vesicles in synaptotagmin mutants of Caenorhabditis elegans. Nature. 1995; 378:196–199. DOI: 10.1038/378196a0 [PubMed: 7477324]
16. Reist NE, et al. Morphologically docked synaptic vesicles are reduced in synaptotagmin mutants of Drosophila. J Neurosci. 1998; 18:7662–7673. [PubMed: 9742137]
17. Siksou L, et al. A common molecular basis for membrane docking and functional priming of synaptic vesicles. Eur J Neurosci. 2009; 30:49–56. DOI: 10.1111/j.1460-9568.2009.06811.x [PubMed: 19558619]
18. Liu H, Dean C, Arthur CP, Dong M, Chapman ER. Autapses and networks of hippocampal neurons exhibit distinct synaptic transmission phenotypes in the absence of synaptotagmin I. J Neurosci. 2009; 29:7395–7403. DOI: 10.1523/JNEUROSCI.1341-09.2009 [PubMed: 19515907]
19. Poskanzer KE, Marek KW, Sweeney ST, Davis GW. Synaptotagmin I is necessary for compensatory synaptic vesicle endocytosis in vivo. Nature. 2003; 426:559–563. DOI: 10.1038/nature02184 [PubMed: 14634669]
20. van den Bogaart G, et al. Synaptotagmin-1 may be a distance regulator acting upstream of SNARE nucleation. Nat Struct Mol Biol. 2011; 18:805–812. DOI: 10.1038/nsmb.2061 [PubMed: 21642968]
21. Honigmann A, et al. Phosphatidylinositol 4,5-bisphosphate clusters act as molecular beacons for vesicle recruitment. Nat Struct Mol Biol. 2013; 20:679–686. DOI: 10.1038/nsmb.2570 [PubMed: 23665582]
22. Bai J, Tucker WC, Chapman ER. PIP2 increases the speed of response of synaptotagmin and steers its membrane-penetration activity toward the plasma membrane. Nat Struct Mol Biol. 2004; 11:36–44. DOI: 10.1038/nsmb709 [PubMed: 14718921]
23. Li L, et al. Phosphatidylinositol phosphates as co-activators of Ca2+ binding to C2 domains of synaptotagmin 1. J Biol Chem. 2006; 281:15845–15852. DOI: 10.1074/jbc.M600888200 [PubMed: 16595652]
24. Xue M, Ma C, Craig TK, Rosenmund C, Rizo J. The Janus-faced nature of the C(2)B domain is fundamental for synaptotagmin-1 function. Nat Struct Mol Biol. 2008; 15:1160–1168. DOI: 10.1038/nsmb.1508 [PubMed: 18953334]
25. Brewer KD, et al. Dynamic binding mode of a Synaptotagmin-1-SNARE complex in solution. Nat Struct Mol Biol. 2015; 22:555–564. DOI: 10.1038/nsmb.3035 [PubMed: 26030874]
26. Seven AB, Brewer KD, Shi L, Jiang QX, Rizo J. Prevalent mechanism of membrane bridging by synaptotagmin-1. Proc Natl Acad Sci U S A. 2013; 110:E3243–3252. DOI: 10.1073/pnas.1310327110 [PubMed: 23918375]
27. Zhou Q, et al. Architecture of the synaptotagmin-SNARE machinery for neuronal exocytosis. Nature. 2015; 525:62–67. DOI: 10.1038/nature14975 [PubMed: 26280336]
28. Zhou A, Brewer KD, Rizo J. Analysis of SNARE complex/synaptotagmin-1 interactions by one-dimensional NMR spectroscopy. Biochemistry. 2013; 52:3446–3456. DOI: 10.1021/bi400230u [PubMed: 23617808]
29. Martens S, Kozlov MM, McMahon HT. How synaptotagmin promotes membrane fusion. Science. 2007; 316:1205–1208. DOI: 10.1126/science.1142614 [PubMed: 17478680]
30. Lynch KL, et al. Synaptotagmin-1 utilizes membrane bending and SNARE binding to drive fusion pore expansion. Mol Biol Cell. 2008; 19:5093–5103. DOI: 10.1091/mbc.E08-03-0235 [PubMed: 18799625]
31. Hui E, Johnson CP, Yao J, Dunning FM, Chapman ER. Synaptotagmin-mediated bending of the target membrane is a critical step in Ca(2+)-regulated fusion. Cell. 2009; 138:709–721. DOI: 10.1016/j.cell.2009.05.049 [PubMed: 19703397]
32. Schaub JR, Lu X, Doneske B, Shin YK, McNew JA. Hemifusion arrest by complexin is relieved by Ca2+-synaptotagmin I. Nat Struct Mol Biol. 2006; 13:748–750. DOI: 10.1038/nsmb1124 [PubMed: 16845390]
33. Heuser JE, Reese TS. Evidence for recycling of synaptic vesicle membrane during transmitter release at the frog neuromuscular junction. J Cell Biol. 1973; 57:315–344. [PubMed: 4348786]

34. Watanabe S, et al. Ultrafast endocytosis at mouse hippocampal synapses. Nature. 2013; 504:242–247. DOI: 10.1038/nature12809 [PubMed: 24305055]
35. Young SM Jr, Neher E. Synaptotagmin has an essential function in synaptic vesicle positioning for synchronous release in addition to its role as a calcium sensor. Neuron. 2009; 63:482–496. DOI: 10.1016/j.neuron.2009.07.028 [PubMed: 19709630]
36. Nishiki T, Augustine GJ. Dual roles of the C2B domain of synaptotagmin I in synchronizing Ca2+-dependent neurotransmitter release. J Neurosci. 2004; 24:8542–8550. DOI: 10.1523/JNEUROSCI.2545-04.2004 [PubMed: 15456828]
37. Gerber SH, Rizo J, Sudhof TC. The top loops of the C(2) domains from synaptotagmin and phospholipase A(2) control functional specificity. J Biol Chem. 2001; 276:32288–32292. DOI: 10.1074/jbc.C100108200 [PubMed: 11447211]
38. Schneggenburger R, Neher E. Presynaptic calcium and control of vesicle fusion. Curr Opin Neurobiol. 2005; 15:266–274. DOI: 10.1016/j.conb.2005.05.006 [PubMed: 15919191]
39. Binz T, et al. Proteolysis of SNAP-25 by types E and A botulinal neurotoxins. J Biol Chem. 1994; 269:1617–1620. [PubMed: 8294407]
40. Schiavo G, et al. Tetanus and botulinum-B neurotoxins block neurotransmitter release by proteolytic cleavage of synaptobrevin. Nature. 1992; 359:832–835. DOI: 10.1038/359832a0 [PubMed: 1331807]
41. Chen YA, Scales SJ, Scheller RH. Sequential SNARE assembly underlies priming and triggering of exocytosis. Neuron. 2001; 30:161–170. [PubMed: 11343652]
42. Chernomordik LV, Kozlov MM. Protein-lipid interplay in fusion and fission of biological membranes. Annu Rev Biochem. 2003; 72:175–207. DOI: 10.1146/annurev.biochem.72.121801.161504 [PubMed: 14527322]
43. Xu J, Pang ZP, Shin OH, Sudhof TC. Synaptotagmin-1 functions as a Ca2+ sensor for spontaneous release. Nat Neurosci. 2009; 12:759–766. DOI: 10.1038/nn.2320 [PubMed: 19412166]
44. Rosenmund C, Stevens CF. Definition of the readily releasable pool of vesicles at hippocampal synapses. Neuron. 1996; 16:1197–1207. [PubMed: 8663996]
45. Min D, et al. Mechanical unzipping and rezipping of a single SNARE complex reveals hysteresis as a force-generating mechanism. Nat Commun. 2013; 4:1705.doi: 10.1038/ncomms2692 [PubMed: 23591872]
46. Jackman SL, Regehr WG. The Mechanisms and Functions of Synaptic Facilitation. Neuron. 2017; 94:447–464. DOI: 10.1016/j.neuron.2017.02.047 [PubMed: 28472650]
47. Lois C, Hong EJ, Pease S, Brown EJ, Baltimore D. Germline transmission and tissue-specific expression of transgenes delivered by lentiviral vectors. Science. 2002; 295:868–872. DOI: 10.1126/science.1067081 [PubMed: 11786607]

Europe PMC Funders Author Manuscripts

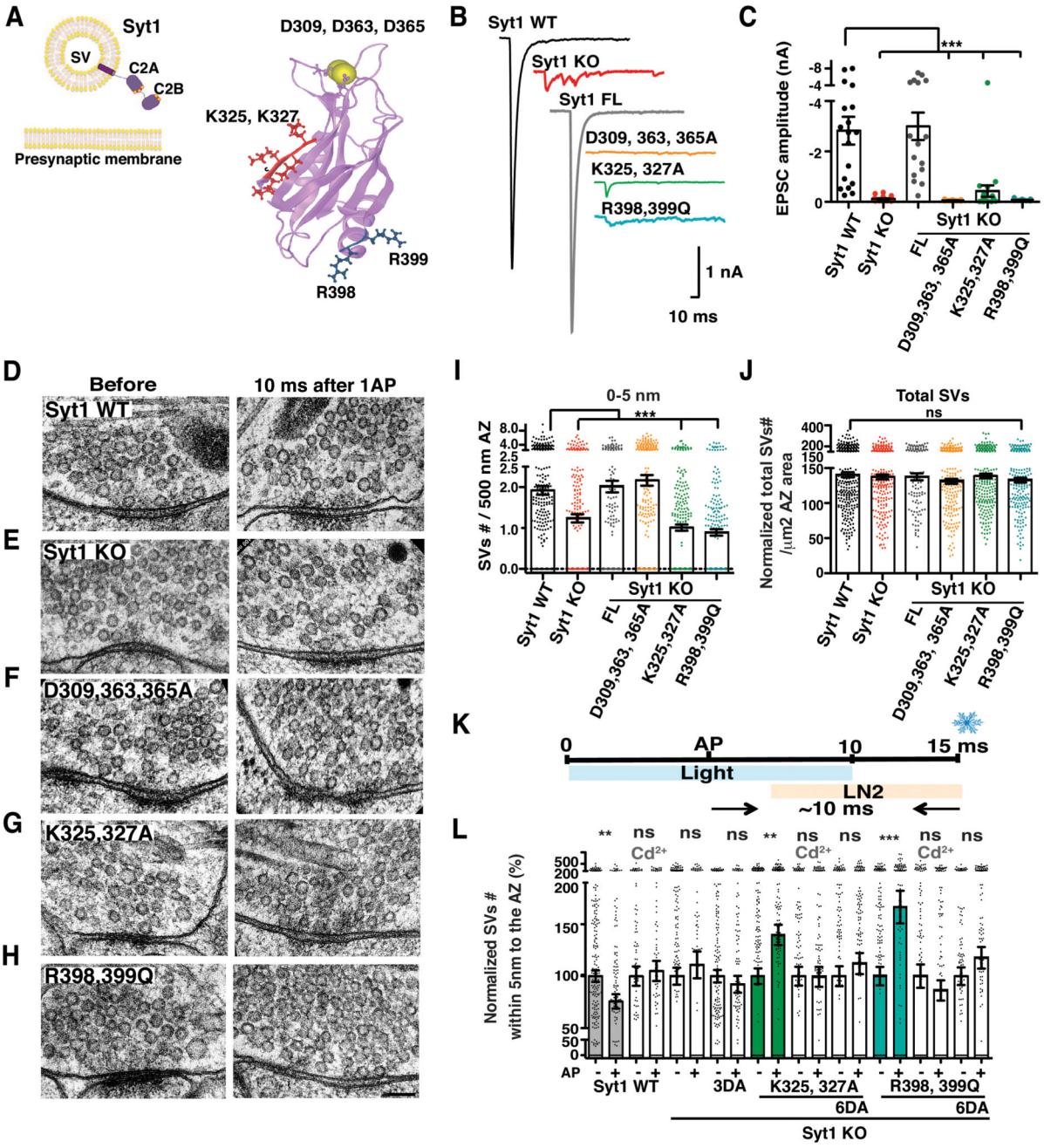

Fig. 1. Syt1 mediates dynamic membrane attachment via its C_2B domain

(A) Schematic illustration of synaptic vesicle (SV), Synaptotagmin1 (Syt1) and plasma membrane. Ribbon diagrams of the Syt1 C_2 B domain. Mutated residues are shown including Ca^{2+} binding site (D309, D363, D365) on the top, polybasic region (K324-K327; red) on the side, and R398, 399 at the bottom (blue) of the C_2B domain. **(B)** Representative evoked autaptic excitatory postsynaptic current (EPSC) traces of hippocampal Syt1 WT, KO and KO neurons rescued with wild-type Syt1 FL (full length) and mutants. Depolarization artifacts and action potentials were blanked. **(C)** Averaged EPSC amplitudes. **(D, E, F, G, H)**

Europe PMC Funders Author Manuscripts

Representative electron micrographs of synapses from Syt1 WT, KO and KO rescued with mutants before and 10 ms after single action potential (AP) stimulation. Scale bar: 100 nm **(I)** Averaged vesicle number within 5 nm of the AZ. Numbers were normalized to the active zone (AZ) lengths. **(J)** Averaged total number of SVs in the presynaptic terminal. Numbers were normalized to the synapse areas. **(K)** Experimental scheme for light stimulation protocol. A pulse of blue light (10 ms) is used to evoke APs, which is generated approximately 5 ms after light onset. A freezing point of 15 ms after light onset was selected as most of the events could be captured approximately 10 ms after AP. LN2: liquid nitrogen. **(L)** Averaged vesicle number within 5 nm to the AZ before and after AP. Data were normalized to AZ length and its resting condition. 3DA indicates mutations in the Ca^{2+} binding site of the C_2B domain (D309, 363, 365A); 6DA indicates mutations in both Ca^{2+} binding sites of the C_2A and C_2B domains. (C_2A: D178, 230, 232A; C_2B: D309, 363, 365A). In (C), n represents the number cells analyzed. In (I, J, L), n represents the number of electron micrographs (synapses) analyzed. Data were obtained from cultured neuron from at least 3 independent cultures and shown as mean ± SEM. In (C, I, J), statistical significance was assessed by Kruskal-Wallis ANOVA test followed by Dunn's multiple comparison test. In (L), Mann-Whitney test was used. ***$p < 0.001$; **$p < 0.01$; ns: not significant. For detailed numbers before normalization, the number of electron micrographs and statistical analysis see Supplementary Table 1A, B, C.

Europe PMC Funders Author Manuscripts

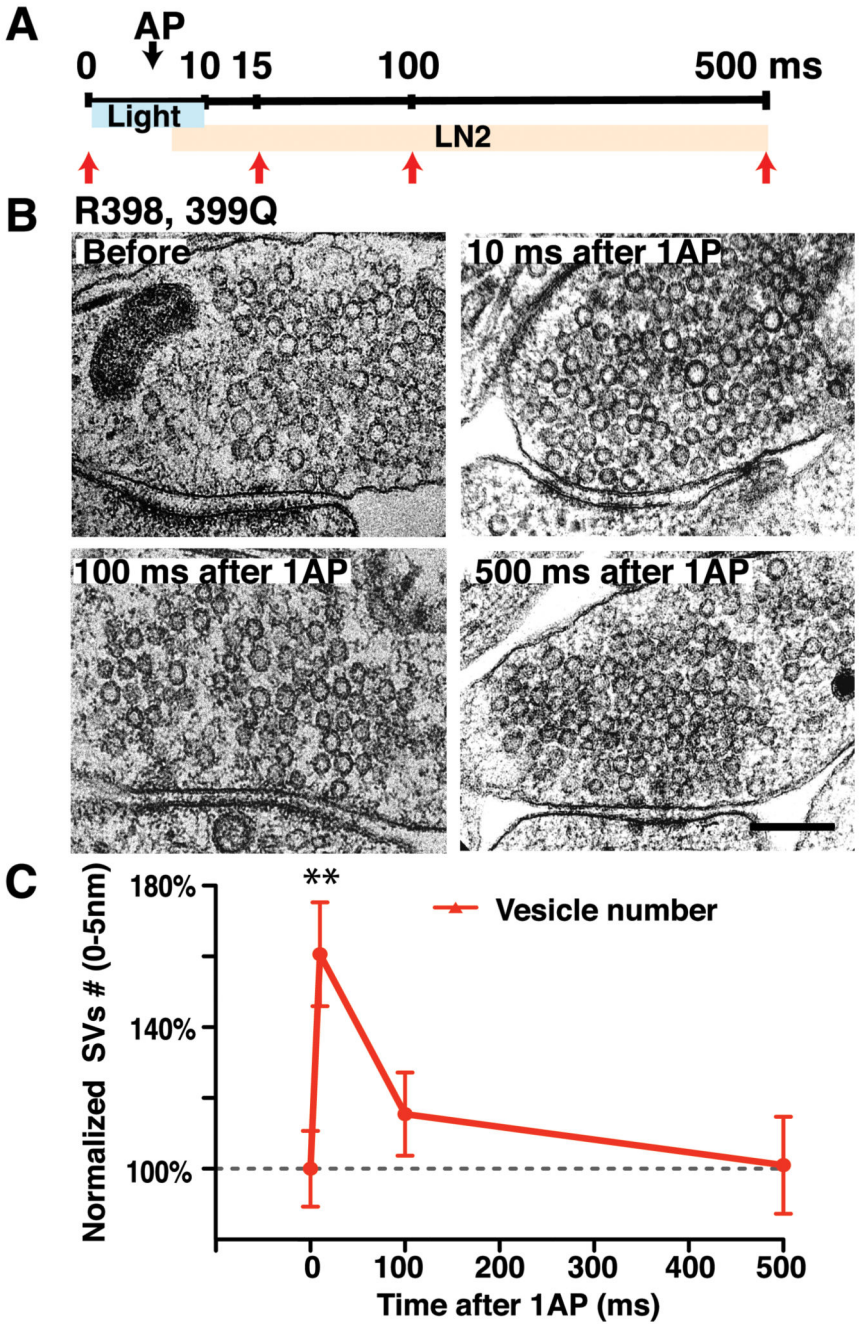

Fig. 2. Activity dependent Syt1 docking is transient and reversible

(A) Experimental scheme for light stimulation protocol. A pulse of blue light (10 ms) is used to evoke single AP. 10, 100, 500 ms time points are used to captured SV dynamics after AP. LN2: liquid nitrogen. **(B)** Representative electron micrographs of Syt1 KO rescued with R398, 399Q mutant before and 10, 100 and 500 ms after AP. Scale bar: 200 nm. **(C)** Normalized vesicle number (0-5 nm to the AZ) before (n = 126) and 10, 100, 500 ms after AP (n = 131, 125 and 127; respectively). Number of vesicles were normalized to AZ length and to the resting condition displayed as percentage. n represents the number of electron

micrographs (synapses) analyzed. Data were obtained from neurons from 3 independent cultures and shown as mean ± SEM. Statistical significance was assessed by Mann-Whitney test. **$p < 0.01$. For detailed numbers before normalization, the number of electron micrographs and statistical analysis see Supplementary Table 1D.

Europe PMC Funders Author Manuscripts

Europe PMC Funders Author Manuscripts

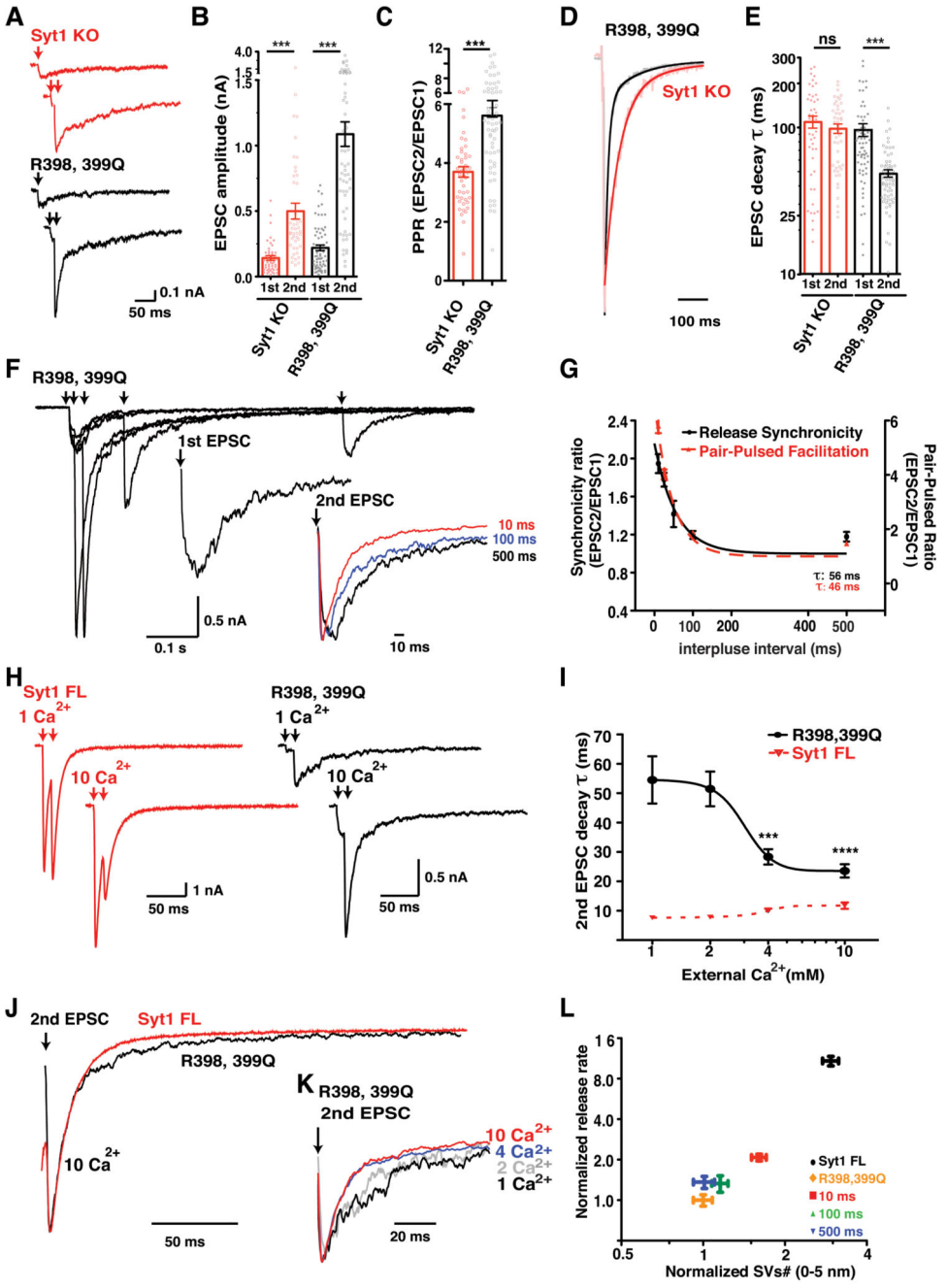

Fig. 3. Ca^{2+}-induced Syt1 docking and release synchronization follow the same rate

(A) Representative single and paired-pulse EPSCs traces (10 ms apart) of autaptic neurons from Syt1 KO (red) and KO rescued with R398, 399Q mutant (black). Depolarization artifacts and action potentials were blanked. **(B)** Scatter plot shows averaged EPSC amplitudes (n = 46, 46, 64, 64; respectively). **(C)** Scatter plot shows averaged paired-pulse ratio (PPR) at 100 Hz (n = 46, 64; respectively) **(D)** Representative fit of the decay of the 2nd EPSCs of paired-pulse responses of Syt1 KO (red) and R398, 399Q mutant (black). EPSCs were scaled and fitted with double exponential functions (see method). **(E)** Scatter plot

shows averaged weighted time constant (τ) of the decays of 2nd EPSC (n = 46, 64; respectively). **(F)** Representative traces of paired-pulse responses with various inter-pulse intervals (10, 25, 100, 500 ms) in R398, 399Q mutant. Scaled 1st and 2nd EPSC response at 10 ms (red), ms (blue) and 500 ms (black). **(G)** Release synchronicity ratio (black) and paired-pulse ratio (red) of 1st EPSC and 2nd EPSC in R398, 399Q mutant with 10, 25, (50), 100, 500 ms inter-pulse intervals (n = 34, 51, 17, 49, 47; respectively; see Material and methods). Time course of the release synchronicity (black) and short-term facilitation (red) were obtained by fitting the data points with single-exponential functions. Time constants of exponential fits are shown. **(H)** Representative paired-pulse EPSCs traces (10 ms apart) of Syt1 KO rescued with wild-type full length (FL) (red) and R398, 399Q mutant (black) in the presence of 1 and 10 mM external Ca^{2+}. **(I)** Averaged decay time constant (τ) of the 2nd EPSCs of the paired-pulse responses recorded in the presence of 1, 2, 4 and 10 mM external Ca^{2+} in Syt1 FL (red; n = 31, 31, 31, 28) or R398, 399Q (black; n = 36, 39, 41, 27) rescued Syt1 KO neurons. Data were fitted with nonlinear logistic Hill equation. **(J)** Normalized traces of 2nd EPSC of the paired-pulse responses in Syt1 FL (red) or R398, 399Q mutant (black) rescued neurons. **(K)** Normalized 2nd EPSC of the paired-pulse responses in R398, 399Q mutant in the presence of 1 (black), 2 (grey), 4 (blue) and 10 (red) mM external Ca^{2+}. **(L)** Correlation of SV number within 0-5 nm to the AZ and release rate of the 2nd EPSC in the paired-pulse responses. Data were normalized to the resting condition of R398, 399Q mutant. n represents the number cells analyzed. Data were obtained from neurons from at least 3 independent cultures and shown as mean ± SEM. Statistical significance was assessed by student t-test or Mann-Whitney test. ***p < 0.001; ns: not significant. For detailed numbers and statistical analysis, see Supplementary Table 1E-K.

Europe PMC Funders Author Manuscripts

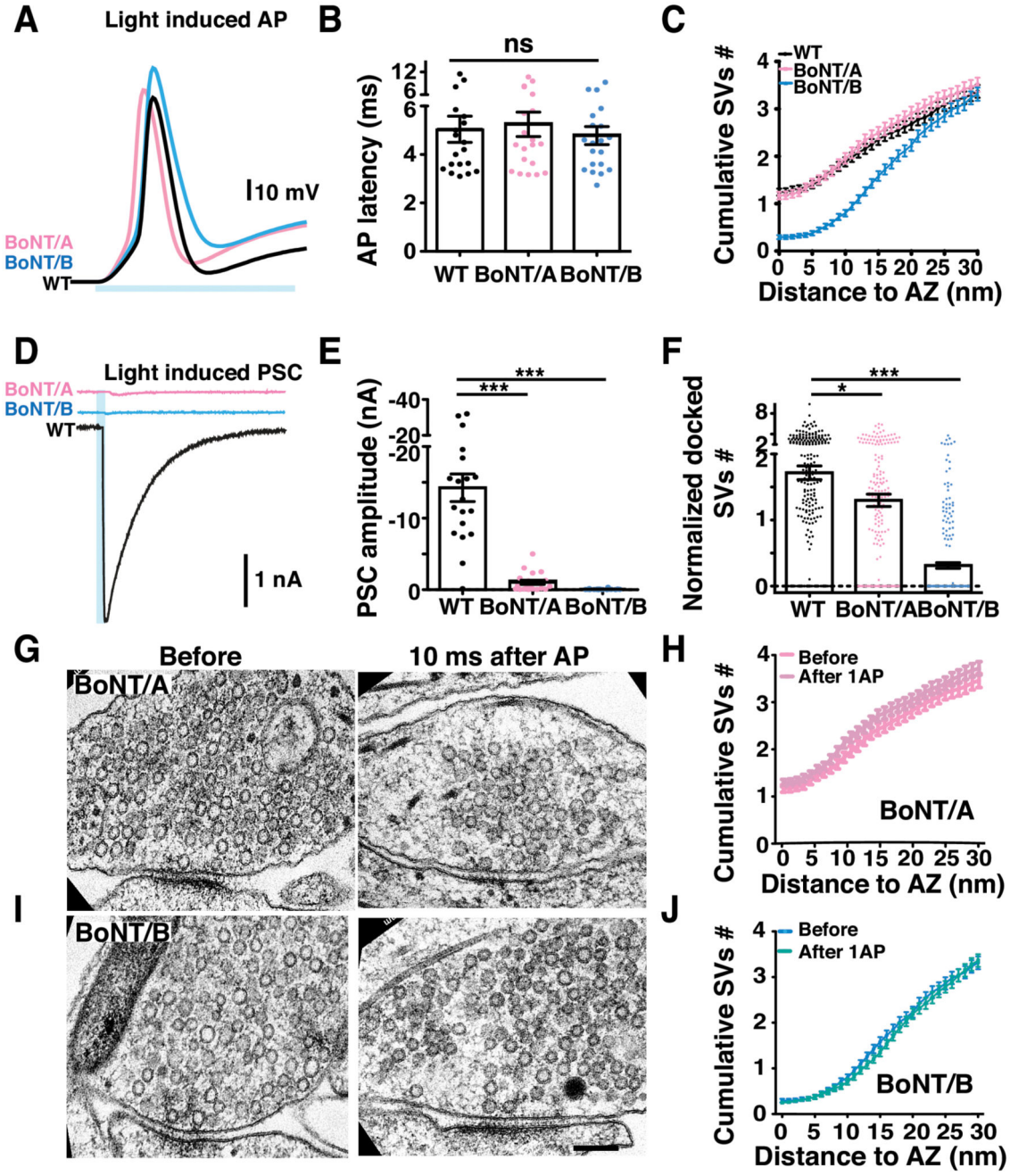

Fig. 4. Ca^{2+}-induced Syt1 docking requires assembly of SNARE complex

(A) Representative AP traces of WT (black), BoNT/A (pink) or BoNT/B (blue) treated WT mass-cultured neurons elicited by a pulse of light (10 ms; light blue). Data were obtained from recordings in current-clamp mode **(B)** Scatter plot shows averaged latency for AP generation (n = 19, 20, 20; respectively) **(C)** Cumulative distribution of the SVs **(D)** Representative postsynaptic currents (PSC) of WT (black) BoNT/A (pink) or BoNT/B (blue) treated WT neurons triggered by a pulse of light (10 ms; light blue). Responses were subtracted with the ChR2 photocurrents obtained by blocking the PSC current with

extracellular solution containing 3 μM NBQX and 30 μM bicuculline (n = 19, 20, 20; respectively) **(E)** Scatter plot shows averaged PSC amplitudes (n = 19, 20, 20; respectively) (**F)** Normalized docked vesicle number. Data were normalized to the AZ lengths. **(G)** Representative electron micrographs of BoNT/A or **(I)** BoNT/B-treated WT synapses before and 10 ms after AP. Scale bar: 100 nm. **(H)** Cumulative distributions of vesicles of BoNT/A treated WT mass-cultured neurons before (n = 206) and after 1AP (n = 224) or of **(J)** BoNT/B treated neurons before (n = 229) and after AP (n = 201). In (B, E) n represents the number cells analyzed. In (C, F, H, J), n represents the number of electron micrographs (synapses) analyzed. Data were obtained from neurons from at least 3 independent cultures and are shown as mean ± SEM. Statistical significance was assessed by Kruskal-Wallis ANOVA test followed by Dunn's multiple comparison test. ***$p < 0.001$; *$p < 0.05$; ns: not significant. For detailed numbers and statistical analysis, see Supplementary Table 1 L, M.

Europe PMC Funders Author Manuscripts